Supplemental Information

Roadside air pollution and secondary organic aerosol seasonal trends from an oxidation flow reactor in Seoul

*Gyutae Park [a], Seokwon Kang [b], Min-Suk Bae [c], Yunsung Lim [d], Chan-Soo Jeon [e], Taehyoung Lee [b]**

[a] *Air Pollution Engineering Division, Climate and Air Quality Research Department, National Institute of Environmental Research, Incheon 22689, Republic of Korea*

[b] *Department of Environmental Science, Hankuk University of Foreign Studies, Yongin 17035, Republic of Korea*

[c] *Department of Environmental Engineering, Mokpo National University, Muan 58554, Republic of Korea*

[d] *Transportation Pollution Research Center, National Institute of Environmental Research, Incheon 22689, Republic of Korea*

[e] *Korea Institute of Civil Engineering and Building Technology, Goyang, 10223, Republic of Korea*

*Corresponding author. Tel.: (+82)-31-330-4039

E-mail address: thlee@hufs.ac.kr

Table. S1 Seasonal roadside information during measurement

	Winter	Spring	Summer	Fall
Period	1/28/2019–2/08/2019 *Korean New Year (KNY): 2/02/2019 00 – 2/07 00	04/15/2019–27/04/2019	07/09/2019–07/16/2019	09/09/2019–09/19/2019 *Korean Thanksgiving Day (KTD): 9/12/2019 00 – 9/16/2019 00
T (°C)	–3.9 ± 4.9	14.1 ± 4.7	24.8 ± 3.3	23 ± 3.3
RH (%)	47.3 ± 17	67.5 ± 21.6	67.7 ±15.7	64.3 ± 20.2
Traffic Volume (# day^{-1})[a]	67,279 ± 6,683	72,966 ± 1,975	70,028 ± 3,232	66,949 ± 5,554
% of gasoline [b]	54% 36,901 ± 4,480	46% 34,885± 1,137	43% 31,950 ± 1,736	46% 32,033 ± 1,254
% of diesel [c]	36% 25,868 ± 7,685	45% 33,212 ± 2,572	46% 32,976 ± 3,714	45% 30,471 ± 5,491
% of LPG [d]	10% 4,510 ± 1,234	9% 4,868 ± 563	11% 5,102 ± 486	9% 4,446 ± 382
Traffic Speed (km $hour^{-1}$)[e]	69.2 ± 11.9	69.3 ± 1.4	64.8 ± 6.9	63.9 ± 7.2

[a,e] The total volume and average speed of traffic were measured by HD Digital Wave Radar(smart Sensor HD Model 126, Wavetronix, Provo, UT, USA), [b–d] the video watch analysis was applied to 6 min in an hour day the interval of ten minutes and calculated them using the statistical extraction method with traffic volume (# $hour^{-1}$). This approach was followed by Park et al. (2021a), who conducted the tunnel project in the same location with the same traffic instrument. [d)] for taxi vehicles.

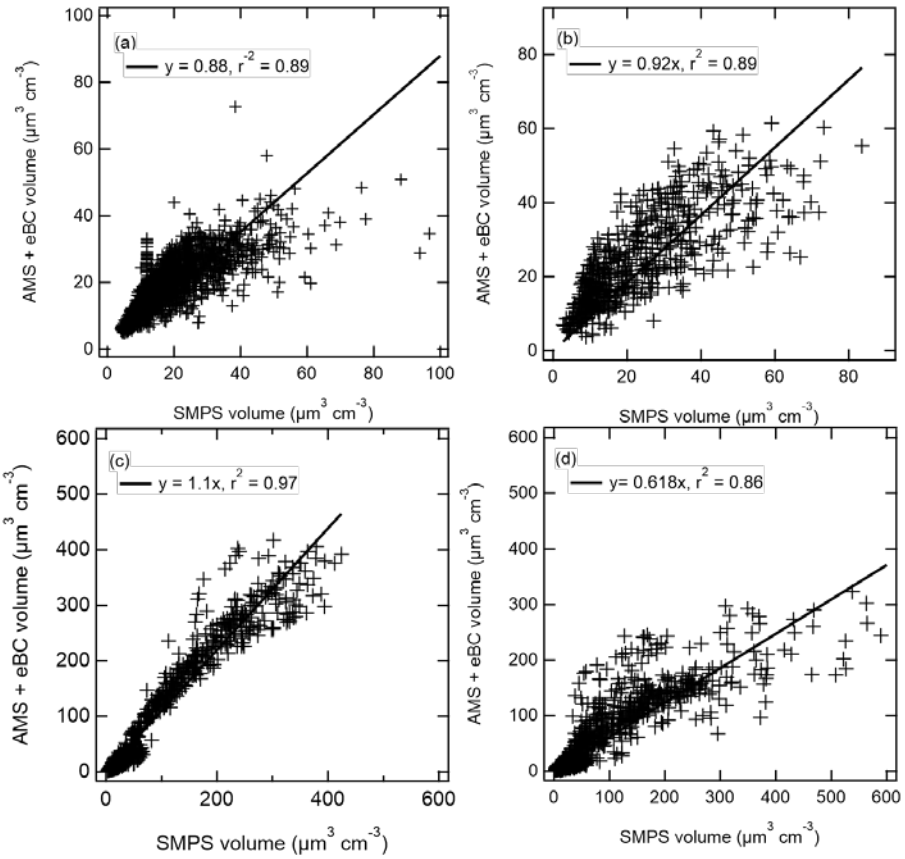

Fig. S1. Scatter plot of roadside and OFR aerosol volume result from AMS plus eBC vs. SMPS with regression line. (a), (b) and (C) were applied to the default CE = 1. (d) was calculated using composition-dependent collection efficiency (CDCE) as Middlebrook et al. (2012). Aerosol densities of 1.75 g cm^{-3} for nitrate, sulfate and ammonium, 1.52 g cm^{-3} for chloride, 1.77 g cm^{-3} for eBC (Ahlberg et al., 2019; Park et al., 2004; Palm et al., 2016). A density of organic (unit: cm^{-3}) was estimated based on the improved elemental composition of [12 + 1*(H/C) + 16*(O/C)]/[7+5*(H/C) + 4.15*(O/C)] (Canagaratna et al., 2015; Kuwata et al., 2012).

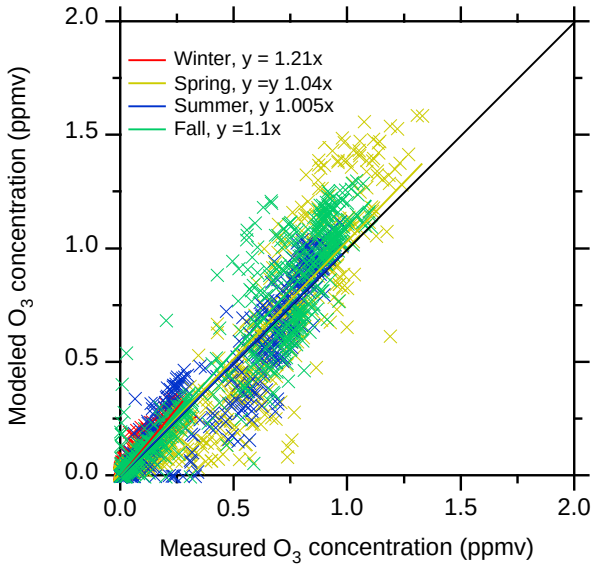

Fig. S2. Comparison of modeled O_3 concentration from photochemical model and measured O_3 concentration after OFR in seasons**.**

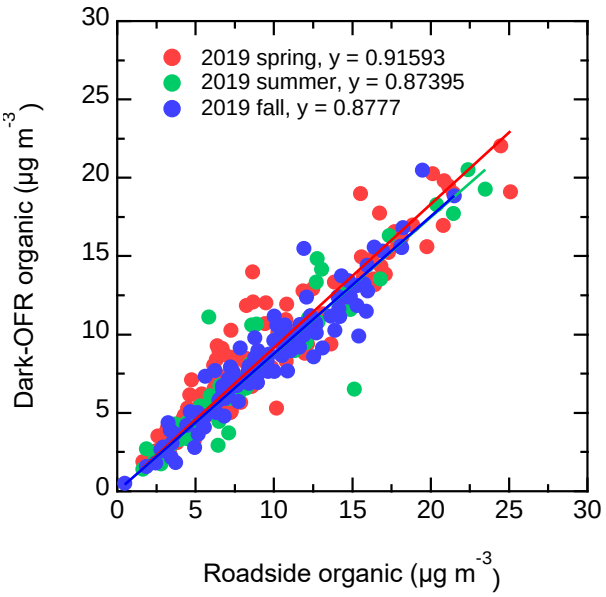

Fig. S3. Relationship between the organic after OFR inside 0% lamp intensity and roadside organic. The winter season wasn`t conducted of dark-OFR, so we applied the average value 0.88919 of other seasons.

Section S1. Morning hour SOA estimation (Fig. S4, Equation S1–S3, Table S2–4)

The purpose of this method is to investigate the seasonal trend in the contribution levels of major component groups among the secondary organic aerosols (SOA) formed in the morning hours (9:30–11:30) on the roadside. Since the concentration of anthropogenic volatile organic compounds (AVOCs) was not measured in this study, the results of the tunnel project conducted previously in the same location were utilized. Since the measurements of the tunnel project were conducted in winter (January) and spring (April) at the same time as this project, the data show consistency. Likewise, for measurements in the fall (September), the SOA components were measured using a proton transfer reaction mass spectrometry (PTR-MS, Iconic), so the measurement hours are the same. However, in the case of summer (July), data from the summer (July) 2018 was used, and data were matched only for overlapping days of the week (Table S2). Fig. S4 shows the pattern of traffic volume during the study period. The average traffic volume from July 28 to August 6, 2018 was 70,328 ± 856 (vehicles day^{-1}), which does not show a significant difference from 70,025 ± 3,232 (vehicles day^{-1}), the traffic volume during the summer measurement period of this study. Thus, it is thought that there was no significant change in the pollutants from motor vehicle emissions.

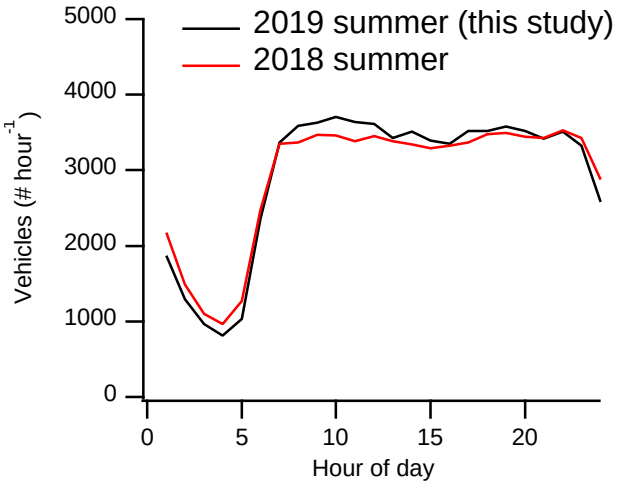

Fig. S4. Hourly pattern of average traffic volume (# $hour^{-1}$) in 2019 and 2018 summer projects. The traffic volumes were measured by HD Digital Wave Radar (smart Sensor HD Model 126, Wavetronix, Provo, UT, USA).

Table. S2. The result of anthropogenic volatile organic compounds (AVOCs): winter, spring, and fall were the same period, and the summer result was part of the 2018 summer project.

Unit : μg m^{-3}

Season	Benzene	Toluene	Ethylbenzene	*m,p*-xylene	*o*-xylene
Winter	4.3 ± 1.2	10.3 ± 8.2	1.4 ± 1-1	1.9 ± 1.3	0.7 ±0.5
Spring	3.1 ± 0.8	20.6 ± 11.9	5.7 ± 3.7	5.8 ± 3.5	2 1.2
Summer 2018	3.7 ± 2.0	16.3 ± 8.4	6.8 ± 3.7	5.9 ±2.9	4.8 ± 2.2
Fall	2.3 ± 0.7	2.1± 1.1		1.8 ± 0.9[a)]	
[a)] The sum of ethylbenzene and *m,p,o*-xylene					

Biogenic VOCs (BVOCs) have been reported to be closely associated with temperature and photosynthetically active radiation (PAR) (Alves et al., 2016; Seco et al., 2015; Warneke et al., 2010). Therefore, in this study, referring to the method of Saha et al. (2018), using the result values of BVOCs measured using PTR-MS during the fall season, the formula proposed by Guenther et al. (1995) was applied to derive the seasonal concentration of BVOCs with respect to temperature and PAR. In the equations S1–S3, c_T is a function of temperature, and c_L is a function of PAR, and since radiation is not measured in this study, the value of PAR was assumed to be 1.

$$\text{Real BVOCs}_\text{i}\text{conc} = \text{base conc (fall)} \times c_T \times c_L \quad \text{(S1)}$$

Isoprene

$$c_T = \frac{e^{(37.711-0.398570815\times dT)}}{1+e^{(91.301-dT)}}, \qquad dT = \frac{28668.514}{K} \quad \text{(S2)}$$

Monoterpenes, sesquiterpene

$$c_T = e^{(0.09\times(K-303))} \quad \text{(S3)}$$

Among the roadside organic, for calculation of semi-volatile organic compounds (SVOCs) and intermediate organic compounds (IVOCs) production, hydrocarbon-like organic aerosol (HOA) factor of the positive matrix factorization (PMF) approach was used (Paatero and Tapper, 1994). The PMF in this study was applied the Multilinear Engine 2 solver (ME-2, Paatero, 2000) controlled within the Source Finder software (SoFi Pro 8.0.4) toolkit for Igor pro 8 (Canonaco et al., 2013, 2015, 2021; Crippa et al., 2014; Paatero, 2000). However, in this study, because source groups other than HOA were not considered, PMF was run through a comprehensive unconstrained run under the condition of a-value 0. The HOA profile extracted

in this way was compared with representative tracer ions, gases, and eBC in terms of the Pearson correlation coefficient (r). In addition, the HOA profile was also compared with the HOA profile of Crippa et al. (2013) provided from the high resolution AMS spectral database for final decision.

HOA is related to fossil fuel emissions such as motor vehicles, and typical mass-to-charge ratios (*m/z*) in AMS database are 41, 43, 55, and 57, showing strong signals for $C_3H_5^+$, $C_3H_7^+$, $C_4H_7^+$, and $C_4H_9^+$ (Crippa et al., 2013; Kim et al., 2018; Sun et al., 2011; Zhang et al., 2005). In addition, HOA shows a high correlation with carbon monoxide (CO), nitrogen oxide (NOx), and equivalent black carbon (eBC), which are representative products of combustion (Lee et al., 2017; Li et al., 2019; Shah et al., 2018). Table S3 shows the results of comparing Pearson's r between the components in this study and unconstrained HOA factor, and for AMS tracer ion, the Pearson's r was 0.5−0.99, confirming a high correlation. Also, the Pearson's r for CO, eBC, and NO_x was 0.34 to 0.78, thus showing a high correlation with the major components of motor vehicle emissions. In the case of NH_3, a correlation of 0.16−0.67 was derived due to the short distance between the sample inlet and the lane and NH_3 emissions from gasoline and LPG vehicles.

Table. S3. Correlation coefficients (Pearson's r) of HOA factor in the roadside of four seasons with AMS tracer ions, gases, particle, and reference profile of HOA.

Compounds	Winter HOA	Spring HOA	Summer HOA	Fall HOA
C_3H_5(*m/z* 41)	0.9	0.62	0.5	0.8
C3H7(*m/z* 43)	0.98	0.92	0.89	0.97
C_4H_7(*m/z* 55)	0.97	0.83	0.77	0.94
C_4H_9(*m/z* 57)	0.99	0.97	0.94	0.99
eBC	0.62	0.39	0.36	0.34
NO_x	0.67	0.78	0.82	0.53
CO	0.42	0.58	0.57	0.41
NH_3	0.16	0.67	0.58	0.42
HOA profile[a)]	0.95	0.92	0.93	0.93
a) This profile was Crippa et al. (2013)`s result that uploaded to the AMS spectral database(http://cires1.colorado.edu/jimenez-group/HRAMSsd/)				

For the final calculation of SOA estimation, Equation 1 in the manuscript was used, and the OH rate constant for each required component and the SOA yield under high NO_x conditions are summarized in Table S4.

Table. S4. Lists of organic groups OH rate constant (25 ℃, molecules cm^{-3}) and SOA yield under high NO_x condition.

Compound	OH rate constant (cm^3 $molec.^{-1}$ s^{-1})	Reference	SOA Yield	Reference
AVOCs				
Benzene	1.2×10^{-12}	Atkinson et al. (2006)	0.281	Ng et al. (2007a)
Toluene	6.05×10^{-12}	Atkinson et al. (2006)	0.08	Ng et al. (2007b)
Ethylbenzene	7×10^{-12}	Atkinson and Arey (2003)	0.072	Yao et al. (2016)
m+p-xylene	1.87×10^{-11}	Atkinson and Arey (2003)	0.08	Ng et al. (2007a)
o-xylene	1.36×10^{-11}	Atkinson and Arey (2003)	1.37E-4	Zhang et al. (2020)
BVOCs				
Isoprene	1×10^{-10}	Atkinson (1997)	0.02	Yao et al. (2016)
Monoterpenes (α-, β-pinene)	6.63×10^{-11}	Atkinson (1997)	0.11	-α -pinene Ng et al. (2007b) β-pinene Sarrafzadeh et al. (2016)
Sesquiterpene (longifolene)	4.8×10^{-11}	Atkinson and Arey (2003)	0.89	Ng et al. (2007b)
S/IVOCs vehicles exhaust				
Gasoline	2.0×10^{-11}	Nault et al. (2018)	0.24	Shah et al. (2020)
Diesel	2.0×10^{-11}	Nault et al. (2018)	0.38	Shah et al. (2020)

Table. S5. Registered vehicles in South Korea in 2019. This result was in supporting information of Park et al. (2021b)

No.	Fuel	South Korea		Seoul	
		Count	Portion	Count	Portion
1	Gasoline	21,921,558	46.3%	1,597,621	51.1%
2	Diesel	19,915,086	42.1%	1,140,532	36.5%
3	Liquefied petroleum gas (LPG)	4,009,460	8.5%	279,713	9.0%
4	Kerosene	2	0.0%	-	-
5	Electric	179,836	0.4%	10,175	0.3%
6	Alcohol	2	0.0%	-	-
7	Compressed natural gas (CNG)	76,294	0.2%	9,607	0.3%
8	Liquefied natural Gas (LNG)	10	0.0%	-	-
9	Hybrid (gasoline + electric)	976,256	2.1%	78,778	2.5%
10	Hybrid (diesel + electric)	1,204	0.0%	31	0.0%
11	Hybrid (LPG + electric)	33,980	0.1%	1,939	0.1%
12	Hybrid (CNG + electric)	654	0.0%	51	0.0%
13	Hybrid (LNG + electric)	-	0.0%	-	-
14	Hydrogen	10,166	0.0%	143	0.0%
15	Others	230,224	0.5%	5,699	0.2%
	Total	47,354,732	100%	3,124,289	100%

Table. S6. Average (± 1σ standard deviation) concentration of gaseous and aerosols on the roadside with comparison data of the monitoring station from the distance of 3.2 km in this site.

	Winter	Spring	Summer	Fall
CO (ppm)	1.49 (± 0.36)	1.83 (±0.63)	1.26 (± 0.6)	1.11 (± 0.38)
CO_2 (ppm)	589 (± 112)	640 (± 143)	605 (± 143)	569 (±113)
NH_3 (ppb)	81.5 (± 28.4)	141.7 (± 50)	94.3 (± 41.3)	62.4 (± 27)
NO_x (ppb)	686 (± 442)	798 (± 499)	407 (± 325)	308 (± 267)
NO / NO_x	0.7	0.8	0.7	0.8
SO_2 (ppb)	7.39 (± 5.66)	9.66 (± 5.71)	6.61 (± 1.63)	1.41 (± 1.04)
O_3 (ppb)	4.35 (± 4.84)	3.45 (± 2.8)	6.26 (± 3.82)	9.63 (± 4.02)
$PM_{AMS+eBC}$ ($\mu g\ m^{-3}$)	30.4 (± 13.1)	38.0 (± 19.8)	31.1 (± 18)	25.3 (± 12.3)
eBC	9.0 (± 6.43)	18.7 (± 12.31)	11.6 (± 8.23)	10.0 (± 7.83)
Organic	10.9 (± 4.8)	9.1 (± 5.2)	8.7(± 4.9)	10.1 (± 4.8)
Nitrate	4.7 (± 3.4)	4.4 (± 3.9)	3.4 (± 3.7)	1.4 (± 2.3)
Sulfate	2.9 (± 2.0)	3.3 (± 2.0	5.0 (± 4.2)	2.5 (± 1.7)
Ammonium	2.5 (± 1.5)	2.4 (± 1.6)	2.4 (± 2.1)	1.2 (± 1.1)
Chloride	0.5 (± 0.3)	0.2 (± 0.2)	0.1 (± 0.1)	0.1 (± 0.1)
Near monitoring station far from 3.2 km classified urban air pollutants in Seoul				
PM_{10} ($\mu g\ m^{-3}$)	59.4	41.3	7.7 [a)]	8.1
$PM_{2.5}$ ($\mu g\ m^{-3}$)	24.9	19.5	8.1 [b)]	11.3
O_3 (ppb)	16.8	30.1	35.2 [c)]	27.7
NO_2 (ppb)	35.5	35.6	9.3 [d)]	16.8
CO (ppm)	0.6	0.5	0.31 [e)]	0.43
SO_2 (ppb)	3.9	3.2	4 [f)]	4
[a-f)] There were loss data period of 7/11/2019 12:00 to 7/16/2019 17:00 in summer. So these data were not comparable with ours result.				

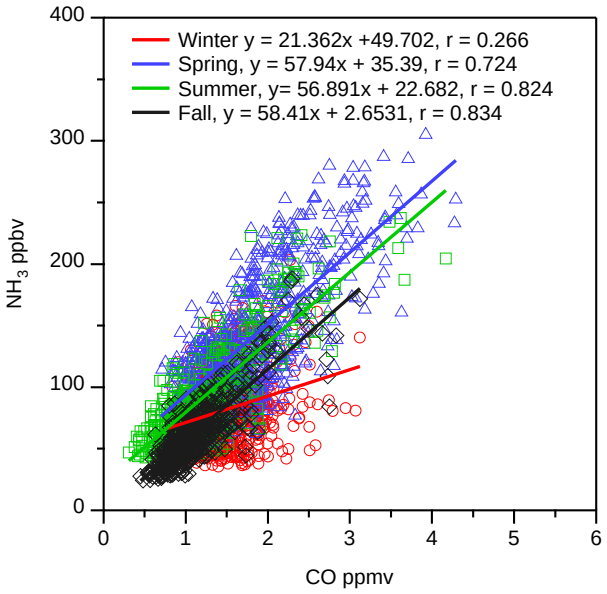

Fig. S5. The Pearson`s correlation coefficients (*r*) between NH_3 (ppb) and CO (ppm) during real-time measurement period.

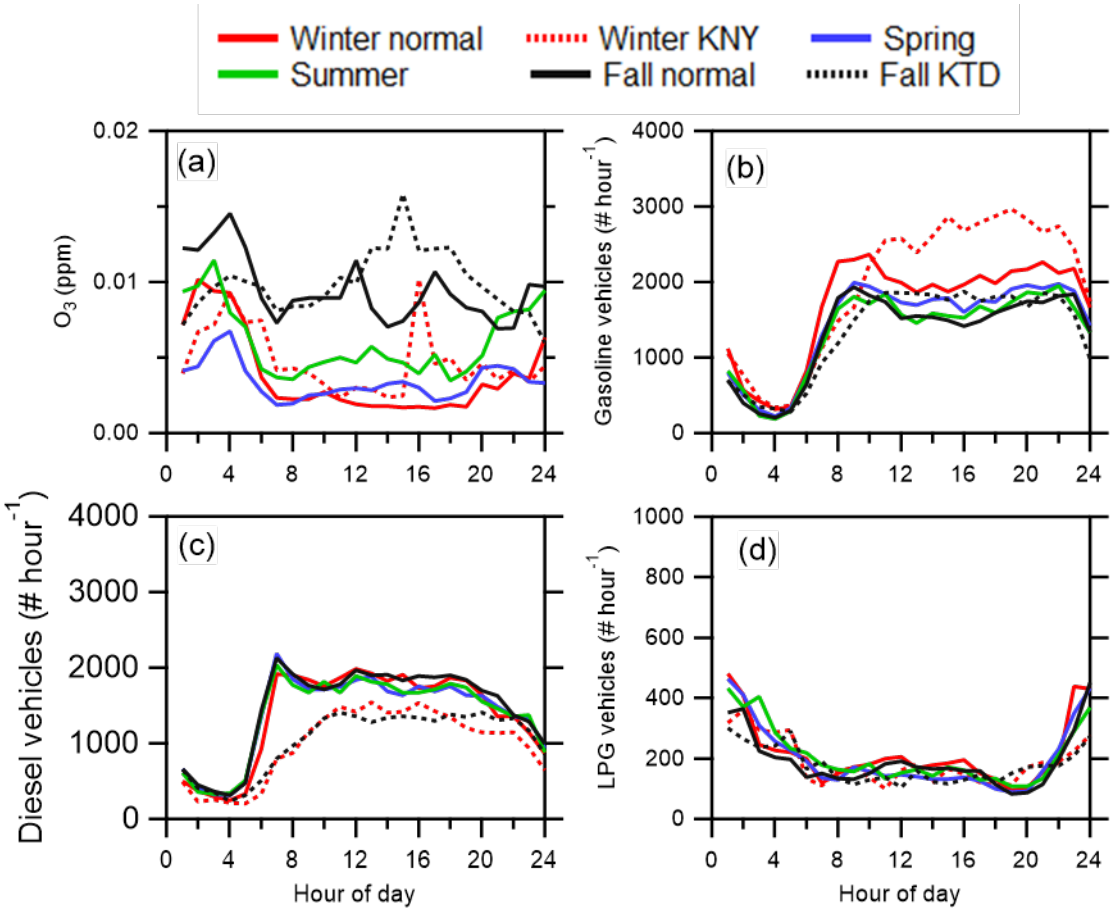

Fig. S6. Diurnal pattern of (a) O_3 and (b−c) average traffic volume of each fuel type (gasoline, diesel, and LPG) in seasons.

Table. S7. Comparison result (± 1σ standard deviation) of normal days and holidays in Korea on the roadside.

compound	Winter		Fall	
	KNY	Winter-normal	KTD	Fall-normal
AMS + eBC ($\mu g\ m^{-3}$)	32.16 (± 11.58)	28.95 (± 14.1)	23.64 (± 10.14)	26.54 (± 13.48)
eBC	8.2 (± 5.34)	9.71 (± 7.17)	6.53 (± 3.62)	12.58 (± 9)
Organic	11.38 (± 4.81)	10.52 (± 4.83)	10.81 (± 4.4)	9.62 (± 5.01)
Nitrate	5.46 (± 3.27)	3.99 (± 3.27)	2.25 (± 3.25)	0.8 (± 0.78)
Sulfate	3.63 (± 2)	2.24 (± 1.68)	2.57 (± 1.74)	2.51 (± 1.61)
Ammonium	2.96 (± 1.55)	2.06 (± 1.4)	1.41 (± 1.42)	0.98 (± 0.67)
Chloride	0.53 (± 0.34)	0.43 (± 0.28)	0.08 (± 0.09)	0.05 (± 0.12)
O_3 (ppb)	4.8 (± 6)	4 (± 3.4)	9.7 (± 3.5)	9.5 (± 4.4)
CO (ppm)	1.47 (± 0.33)	1.51 (± 0.38)	1.01 (± 0.27)	1.19 (± 0.44)
CO_2 (ppm)	575.5 (± 91.5)	600.2 (± 125.7)	531.5 (± 75.3)	596.4 (± 127.8)
SO_2 (ppb)	4.97 (± 2.82)	9.5 (± 6.58)	0.9 (± 0.5)	1.8 (± 1.2)
NO (ppb)	362.3 (± 198.6)	660.1 (± 433.8)	143.8 (± 103)	313.1 (± 254)
NO_2 (ppb)	145.4 (± 55.9)	203.1 (± 94.5)	48.3 (± 34.9)	85.9 (± 56)
NO_x (ppb)	501.3 (± 239.7)	845.7 (± 510.1)	190.2 (± 134.8)	395.3 (± 304.7)
NO/ NO_x	0.69 (± 0.09)	0.75 (± 0.08)	0.75 (± 0.1)	0.77 (± 0.1)
NH_3 (ppb)	91 (± 31.3)	73.3 (± 22.6)	54.8 (± 20)	68 (± 29.9)
Ratio of the truck in diesel vehicles	0.11	0.3	0.09	0.28

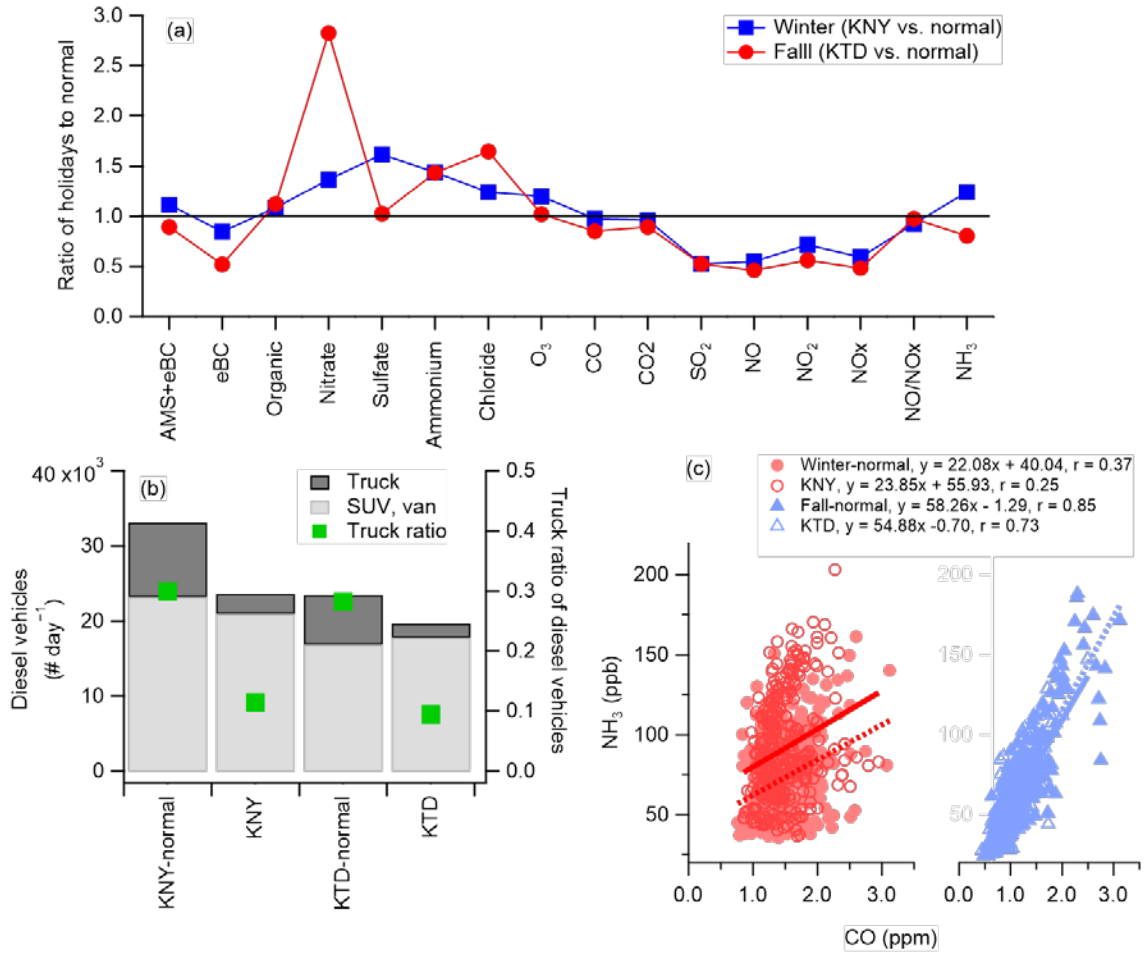

Fig. S7. (a) the ratio of holidays and normal days in gaseous compounds and aerosols. (b) The total volume of diesel vehicle and contribution of categories in diesel vehicles. (c) the comparison of NH_3 and CO in normal days and holidays on winter and fall.

Table. S8. The range of organic and inorganic potential enhancement and photochemical OH· concentration modified OFR in seasons. (The result unit of compound in AMS is μg m^{-3})

Compound	Winter normal (Winter KNY)	Spring	Summer	Fall normal (Fall KTD)
OA_{PE}	0.4−1.5 (0.8−1.6)	28.4−52.3	40.5−57.7	18.1−31.1 (12.1−21.9)
$Nitrate_{PE}$	0.4−1.5 (0.9−1.5)	82.2−141.2	158.6−251.4	165.3−290.8 (126.2−214.9)
$Sulfate_{PE}$	0.2−0.5 (0.1−0.6)	-0.2−0.01	-1.0 − -0.2	-1.6− -0.9 (-1.6 – -0.7)
$Ammonium_{PE}$	-0.3−0.1 (-0.2−0.1)	25.6−43.7	49.9−78.9	42−73.3 (32.2−56.1)
$Chloride_{PE}$	-0.4−0.2 (-0.4−0.2)	0.06−0.1	0.22−0.24	0.1−0.3 (0.03−0.1)
OA_{PE} / $CO_{bkg\text{-}cor}$ (μg m^{-3} ppm^{-1})	1.1−3.4 (1.9−8)	41.2−157.4	89.5−414.7	41.6−151.5 (34.9−77.3)
Photochemical OH· day	0.5—8.4 (0.6—8.5)	0.4−3.3	0.2−4.0	0.2−4.3 (0.2−4.3)
* Negative values meant time difference between direct measurement and OFR measurement				

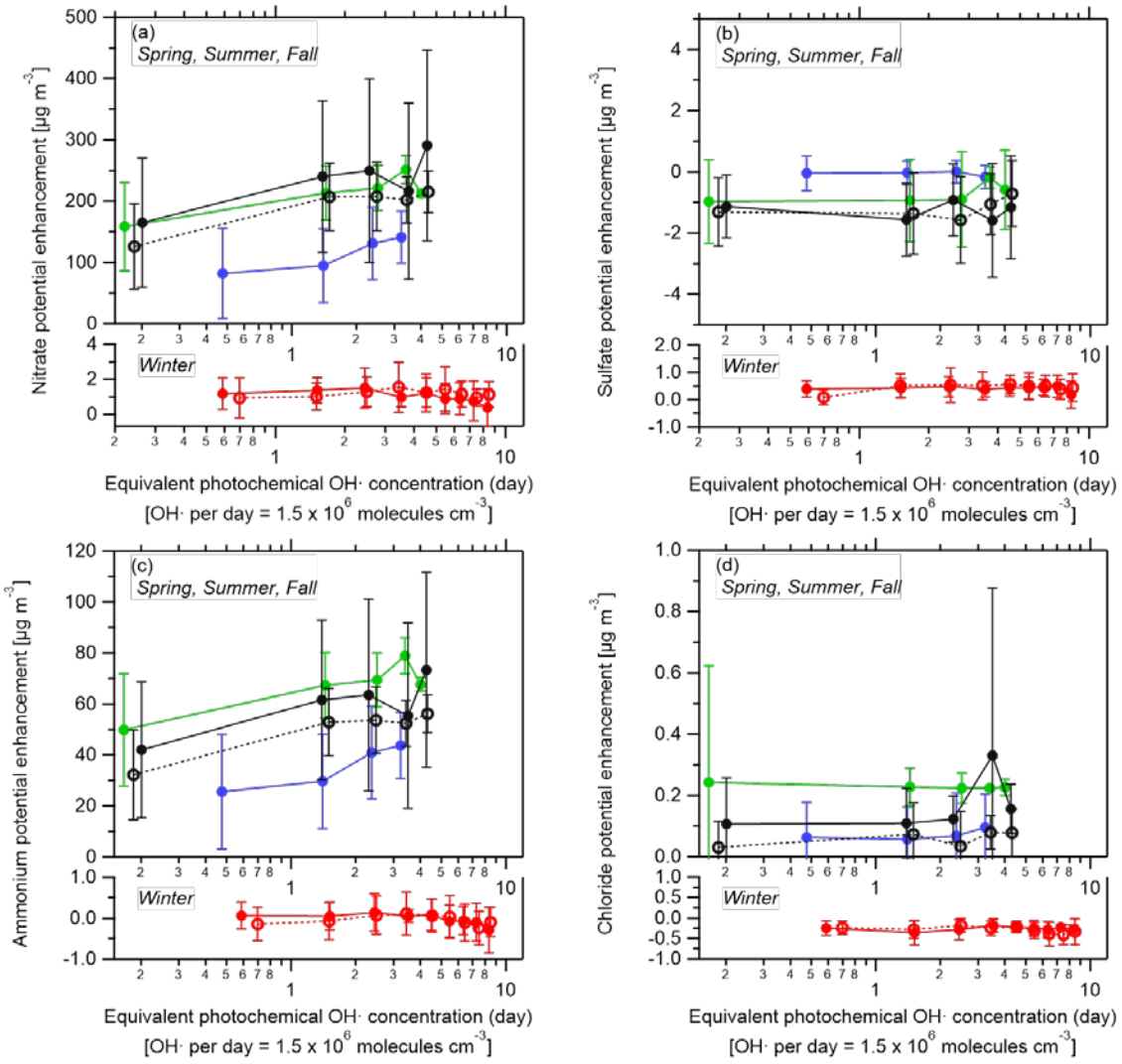

Fig. S8. Seasonal inorganics potential enhancement ($inorganic_{PE}$ = secondary inorganic aerosol formed and corrected in oxidation flow reactor – inorganic corrected in the roadside) by increasing OH· concentration inside the OFR. (a) nitrate. (b) sulfate. (c) ammonium. (d) chloride.

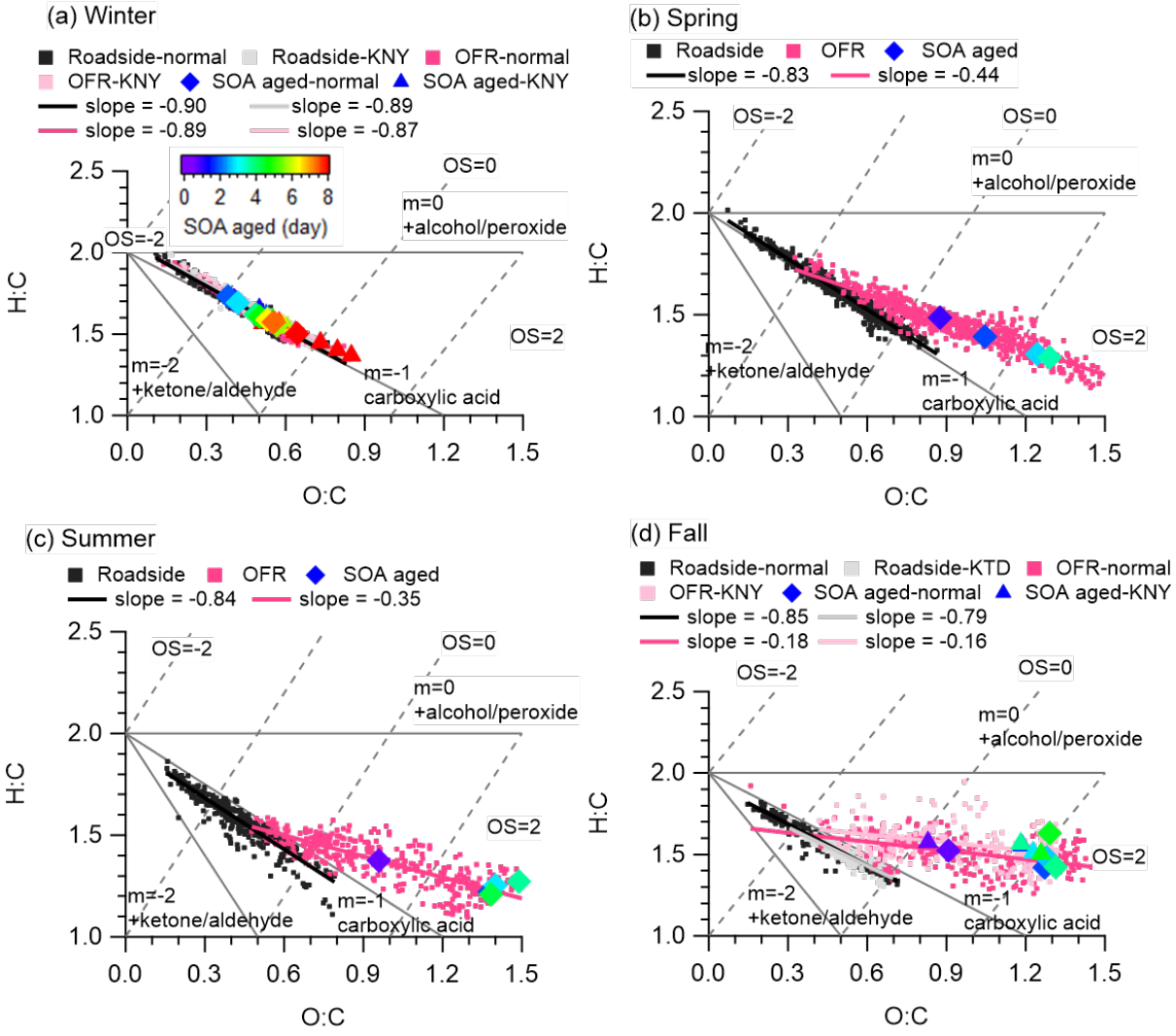

Fig. S9. Van Krevelen diagrams of H/C vs. O/C ratios of organic from roadside and after oxidation by OH·.

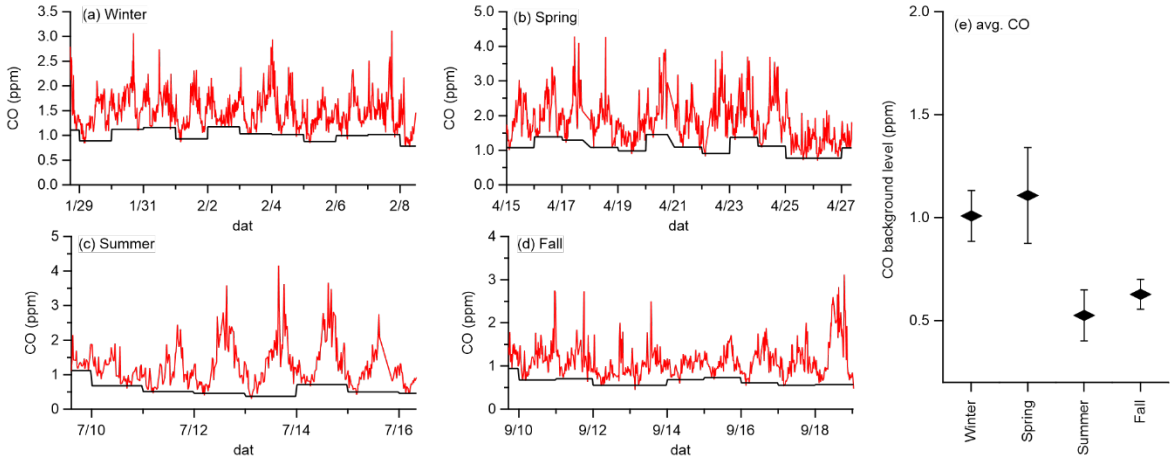

Fig. S10. (a−d) the timeline of CO (red line) and calculated background CO (black line) in seasons. (e) the average concentration of the background CO level on the roadside.

Table. S9. The range of organic, eBC, organic potential enhancement (OA_{PE}), and proportion of the OA_{PE} under ~4.5 $OH\cdot$ day. (The resulting unit of compound is $\mu g\ m^{-3}$)

Compound	Winter		Spring	Summer	Fall	
	KNY	Normal			KTD	Normal
eBC	8.2	9.71	18.7	11.6	6.53	12.58
Organic	11.38	10.52	9.1	8.7	10.81	9.62
OA_{PE}	1.0	1.2	41	47.9	17.9	26.4
Ratio of OA_{PE} to total(organic, eBC, OA_{PE})	5.1%	5.5%	59.6%	70.2%	50.9%	54.3%

REFERENCES

Ahlberg, E., Ausmeel, S., Eriksson, A., Holst, T., Karlsson, T., Brune, W.H., Frank, G., Roldin, P., Kristensson, A., Svenningsson, B., 2019. No Particle Mass Enhancement from Induced Atmospheric Ageing at a Rural Site in Northern Europe. Atmosphere 10, 408. https://doi.org/10.3390/atmos10070408.

Alves, E.G., Jardine, K., Tota, J., Jardine, A., Yãnez-Serrano, A.M., Karl, T., Tavares, J., Nelson, B., Gu, D., Stavrakou, T., Martin, S., Artaxo, P., Manzi, A., Guenther, A., 2016. Seasonality of isoprenoid emissions from a primary rainforest in central Amazonia. Atmos. Chem. Phys. 16, 3903−3925. https://doi.org/10.5194/acp-16-3903-2016.

Atkinson, R., 1997. Gas-phase tropospheric chemistry of volatile organic compounds: 1. Alkanes and alkenes. J. Phys. Chem. Ref. Data 26, 215−290. https://doi.org/10.1063/1.556012.

Atkinson, R., Arey, J., 2003. Gas-phase tropospheric chemistry of biogenic volatile organic compounds: a review. Atmos. Environ. 37, 197−219. https://doi.org/10.1016/s1352-2310(03)00391-1.

Atkinson, R., Baulch, D., Cox, R., Crowley, J., Hampson, R., Hynes, R., Jenkin, M., Rossi, M., Troe, J., Subcommittee, I., 2006. Evaluated kinetic and photochemical data for atmospheric chemistry: Volume II–gas phase reactions of organic species. Atmos. Chem. Phys. 6, 3625−4055. https://doi.org/10.5194/acp-6-3625-2006.

Canagaratna, M.R., Jimenez, J.L., Kroll, J.H., Chen, Q., Kessler, S.H., Massoli, P., Hildebrandt Ruiz, L., Fortner, E., Williams, L.R., Wilson, K.R., Surratt, J.D., Donahue, N.M., Jayne, J.T., Worsnop, D.R., 2015. Elemental ratio measurements of organic compounds using

aerosol mass spectrometry: characterization, improved calibration, and implications. Atmos. Chem. Phys. 15, 253−272. https://doi.org/10.5194/acp-15-253-2015.

Canonaco, F., Crippa, M., Slowik, J., Baltensperger, U., Prévôt, A., 2013. SoFi, an IGOR-based interface for the efficient use of the generalized multilinear engine (ME-2) for the source apportionment: ME-2 application to aerosol mass spectrometer data. Atmos. Meas. Tech. 6, 3649−3661. https://doi.org/10.5194/amt-6-3649-2013.

Canonaco, F., Slowik, J., Baltensperger, U., Prévôt, A., 2015. Seasonal differences in oxygenated organic aerosol composition: implications for emissions sources and factor analysis. Atmos. Chem. Phys. 15, 6993−7002. https://doi.org/10.5194/acp-15-6993-2015.

Canonaco, F., Tobler, A., Chen, G., Sosedova, Y., Slowik, J.G., Bozzetti, C., Daellenbach, K.R., El Haddad, I., Crippa, M., Huang, R.J., Furger, M., Baltensperger, U., Prévôt, A.S.H., 2021. A new method for long-term source apportionment with time-dependent factor profiles and uncertainty assessment using SoFi Pro: application to 1 year of organic aerosol data. Atmos. Meas. Tech. 14, 923−943. https://doi.org/10.5194/amt-14-923-2021.

Crippa, M., Canonaco, F., Lanz, V.A., Äijälä, M., Allan, J.D., Carbone, S., Capes, G., Ceburnis, D., Dall'Osto, M., Day, D.A., DeCarlo, P.F., Ehn, M., Eriksson, A., Freney, E., Hildebrandt Ruiz, L., Hillamo, R., Jimenez, J.L., Junninen, H., Kiendler-Scharr, A., Kortelainen, A.M., Kulmala, M., Laaksonen, A., Mensah, A.A., Mohr, C., Nemitz, E., O'Dowd, C., Ovadnevaite, J., Pandis, S.N., Petäjä, T., Poulain, L., Saarikoski, S., Sellegri, K., Swietlicki, E., Tiitta, P., Worsnop, D.R., Baltensperger, U., Prévôt, A.S.H., 2014. Organic aerosol components derived from 25 AMS data sets across Europe using a consistent ME-2 based source apportionment approach. Atmos. Chem. Phys. 14, 6159−6176. https://doi.org/10.5194/acp-14-6159-2014.

Crippa, M., El Haddad, I., Slowik, J.G., DeCarlo, P.F., Mohr, C., Heringa, M.F., Chirico, R., Marchand, N., Sciare, J., Baltensperger, U., Prévôt, A.S.H., 2013. Identification of marine and continental aerosol sources in Paris using high resolution aerosol mass spectrometry. J. Geophys. Res. Atmos. 118, 1950−1963. https://doi.org/10.1002/jgrd.50151.

Guenther, A., Hewitt, C.N., Erickson, D., Fall, R., Geron, C., Graedel, T., Harley, P., Klinger, L., Lerdau, M., Mckay, W.A., Pierce, T., Scholes, B., Steinbrecher, R., Tallamraju, R., Taylor, J., Zimmerman, P., 1995. A global model of natural volatile organic compound emissions. J. Geophys. Res. Atmos. 100, 8873−8892. https://doi.org/10.1029/94JD02950.

Kim, H., Zhang, Q., Heo, J., 2018. Influence of intense secondary aerosol formation and long-range transport on aerosol chemistry and properties in the Seoul Metropolitan Area during spring time: results from KORUS-AQ. Atmos. Chem. Phys. 18, 7149−7168. https://doi.org/10.5194/acp-18-7149-2018.

Kuwata, M., Zorn, S.R., Martin, S.T., 2012. Using Elemental Ratios to Predict the Density of Organic Material Composed of Carbon, Hydrogen, and Oxygen. Environ. Sci. Technol. 46, 787−794. https://doi.org/10.1021/es202525q.

Lee, B.P., Louie, P.K.K., Luk, C., Chan, C.K., 2017. Evaluation of traffic exhaust contributions to ambient carbonaceous submicron particulate matter in an urban roadside environment in Hong Kong. Atmos. Chem. Phys. 17, 15121−15135. https://doi.org/10.5194/acp-17-15121-2017.

Li, J., Liu, Q., Li, Y., Liu, T., Huang, D., Zheng, J., Zhu, W., Hu, M., Wu, Y., Lou, S., 2019. Characterization of Aerosol Aging Potentials at Suburban Sites in Northern and Southern China Utilizing a Potential Aerosol Mass (Go: PAM) Reactor and HR-ToF-AMS. J. Geophys. Res. Atmos. https://doi.org/10.1029/2018JD029904.

Middlebrook, A.M., Bahreini, R., Jimenez, J.L., Canagaratna, M.R., 2012. Evaluation of Composition-Dependent Collection Efficiencies for the Aerodyne Aerosol Mass Spectrometer using Field Data. Aerosol Sci. Technol. 46, 258−271. https://doi.org/10.1080/02786826.2011.620041.

Nault, B.A., Campuzano-Jost, P., Day, D.A., Schroder, J.C., Anderson, B., Beyersdorf, A.J., Blake, D.R., Brune, W.H., Choi, Y., Corr, C.A., de Gouw, J.A., Dibb, J., DiGangi, J.P., Diskin, G.S., Fried, A., Huey, L.G., Kim, M.J., Knote, C.J., Lamb, K.D., Lee, T., Park, T., Pusede, S.E., Scheuer, E., Thornhill, K.L., Woo, J.H., Jimenez, J.L., 2018. Secondary organic aerosol production from local emissions dominates the organic aerosol budget over Seoul, South Korea, during KORUS-AQ. Atmos. Chem. Phys. 18, 17769−17800. https://doi.org/10.5194/acp-18-17769-2018.

Ng, N., Kroll, J., Chan, A., Chhabra, P., Flagan, R., Seinfeld, J., 2007a. Secondary organic aerosol formation from m-xylene, toluene, and benzene. Atmos. Chem. Phys. 7, 3909−3922. https://doi.org/10.5194/acp-7-3909-2007.

Ng, N.L., Chhabra, P.S., Chan, A.W.H., Surratt, J.D., Kroll, J.H., Kwan, A.J., McCabe, D.C., Wennberg, P.O., Sorooshian, A., Murphy, S.M., Dalleska, N.F., Flagan, R.C., Seinfeld, J.H., 2007b. Effect of NOx level on secondary organic aerosol (SOA) formation from the photooxidation of terpenes. Atmos. Chem. Phys. 7, 5159−5174. https://doi.org/10.5194/acp-7-5159-2007.

Paatero, P., 2000. User's guide for the multilinear engine program "ME2" for fitting multilinear and quasimultilinear models. University of Helsinki, Finland.

Paatero, P., Tapper, U., 1994. Positive matrix factorization: A non-negative factor model with optimal utilization of error estimates of data values. Environmetrics 5, 111−126. https://doi.org/10.1002/env.3170050203.

Palm, B.B., Campuzano-Jost, P., Ortega, A.M., Day, D.A., Kaser, L., Jud, W., Karl, T., Hansel, A., Hunter, J.F., Cross, E.S., Kroll, J.H., Peng, Z., Brune, W.H., Jimenez, J.L., 2016. In situ secondary organic aerosol formation from ambient pine forest air using an oxidation flow reactor. Atmos. Chem. Phys. 16, 2943−2970. https://doi.org/10.5194/acp-16-2943-2016.

Park, C., Song, M., Park, G., Kim, K., Lee, T., Lee, S., Lee, J., Bae, M.-S., 2021a. Real-World Vehicle Emission Rate of Particle Size Distributions Based on Measurement of Tunnel Flow Coefficient. Appl. Sci. 11, 794. https://doi.org/10.3390/app11020794.

Park, G., Kim, K., Park, T., Kang, S., Ban, J., Choi, S., Yu, D.-G., Lee, S., Lim, Y., Kim, S., Mun, S., Woo, J.-H., Jeon, C.-S., Lee, T., 2021b. Primary and secondary aerosols in small passenger vehicle emissions: Evaluation of engine technology, driving conditions, and regulatory standards. Environ. Pollut. 286, 117195. https://doi.org/10.1016/j.envpol.2021.117195.

Park, K., Kittelson, D.B., Zachariah, M.R., McMurry, P.H., 2004. Measurement of Inherent Material Density of Nanoparticle Agglomerates. J. Nanopart Res. 6, 267−272. https://doi.org/10.1023/b:nano.0000034657.71309.e6.

Saha, P.K., Reece, S.M., Grieshop, A.P., 2018. Seasonally Varying Secondary Organic Aerosol Formation From In-Situ Oxidation of Near-Highway Air. Environ. Sci. Technol. 52, 7192−7202. https://doi.org/10.1021/acs.est.8b01134.

Sarrafzadeh, M., Wildt, J., Pullinen, I., Springer, M., Kleist, E., Tillmann, R., Schmitt, S.H., Wu, C., Mentel, T.F., Zhao, D., Hastie, D.R., Kiendler-Scharr, A., 2016. Impact of NOx and OH on secondary organic aerosol formation from β-pinene photooxidation. Atmos. Chem. Phys. 16, 11237−11248. https://doi.org/10.5194/acp-16-11237-2016.

Seco, R., Karl, T., Guenther, A., Hosman, K.P., Pallardy, S.G., Gu, L., Geron, C., Harley, P., Kim, S., 2015. Ecosystem-scale volatile organic compound fluxes during an extreme drought in a broadleaf temperate forest of the Missouri Ozarks (central USA). Glob. Chang. Biol. 21, 3657−3674. https://doi.org/10.1111/gcb.12980.

Shah, R.U., Coggon, M.M., Gkatzelis, G.I., McDonald, B.C., Tasoglou, A., Huber, H., Gilman, J., Warneke, C., Robinson, A.L., Presto, A.A., 2020. Urban Oxidation Flow Reactor Measurements Reveal Significant Secondary Organic Aerosol Contributions from Volatile Emissions of Emerging Importance. Environ. Sci. Technol. 54, 714−725. https://doi.org/10.1021/acs.est.9b06531.

Shah, R.U., Robinson, E.S., Gu, P., Robinson, A.L., Apte, J.S., Presto, A.A., 2018. High-spatial-resolution mapping and source apportionment of aerosol composition in Oakland, California, using mobile aerosol mass spectrometry. Atmos. Chem. Phys. 18, 16325−16344. https://doi.org/10.5194/acp-18-16325-2018.

Sun, Y.-L., Zhang, Q., Schwab, J., Demerjian, K., Chen, W.-N., Bae, M.-S., Hung, H.-M., Hogrefe, O., Frank, B., Rattigan, O., 2011. Characterization of the sources and processes of organic and inorganic aerosols in New York city with a high-resolution time-of-flight aerosol mass apectrometer. Atmos. Chem. Phys. 11, 1581−1602. https://doi.org/10.5194/acp-11-1581-2011.

Warneke, C., de Gouw, J.A., Del Negro, L., Brioude, J., McKeen, S., Stark, H., Kuster, W.C., Goldan, P.D., Trainer, M., Fehsenfeld, F.C., Wiedinmyer, C., Guenther, A.B., Hansel, A., Wisthaler, A., Atlas, E., Holloway, J.S., Ryerson, T.B., Peischl, J., Huey, L.G., Hanks, A.T.C., 2010. Biogenic emission measurement and inventories determination of biogenic emissions in the eastern United States and Texas and comparison with biogenic emission inventories. J. Geophys. Res. Atmos. 115. https://doi.org/10.1029/2009JD012445.

Yao, L., Yang, L., Chen, J., Wang, X., Xue, L., Li, W., Sui, X., Wen, L., Chi, J., Zhu, Y., Zhang, J., Xu, C., Zhu, T., Wang, W., 2016. Characteristics of carbonaceous aerosols: Impact of biomass burning and secondary formation in summertime in a rural area of the North China Plain. Sci. Total Environ. 557−558, 520−530. https://doi.org/10.1016/j.scitotenv.2016.03.111.

Zhang, F., Shang, X., Chen, H., Xie, G., Fu, Y., Wu, D., Sun, W., Liu, P., Zhang, C., Mu, Y., Zeng, L., Wan, M., Wang, Y., Xiao, H., Wang, G., Chen, J., 2020. Significant impact of coal combustion on VOCs emissions in winter in a North China rural site. Sci. Total Environ. 720, 137617. https://doi.org/10.1016/j.scitotenv.2020.137617.

Zhang, Q., Alfarra, M.R., Worsnop, D.R., Allan, J.D., Coe, H., Canagaratna, M.R., Jimenez, J.L., 2005. Deconvolution and Quantification of Hydrocarbon-like and Oxygenated Organic Aerosols Based on Aerosol Mass Spectrometry. Environ. Sci. Technol. 39, 4938−4952. https://doi.org/10.1021/es048568l.